

# A new direct method of continuous unwrapping phase from a single interferogram

V. BEREJNOV<sup>1,\*</sup> AND B. Y. RUBINSTEIN<sup>2</sup>

<sup>1</sup>6575 St. Charles Pl, Burnaby, V5H3W1, Canada

<sup>2</sup>Stowers Institute for Medical Research, 1000 East 50th Street, Kansas City, MO 64110, USA

\*berejnov@gmail.com

Compiled August 1, 2024

A new method recovers the phase difference of interfering wavefronts from a pattern of interference fringes, avoiding the phase discontinuity problem. The method relies on the numerical solution of one-dimensional first-order ordinary differential equations. The solution of each equation allows to compute a corresponding cross section of the two-dimensional phase, leading to the effective recovery of the phase surface. The unwrapping procedure can be performed in each orthogonal direction.

<http://dx.doi.org/10.1364/ao.XX.XXXXXX>

**Introduction.** Recovering the phase profile from a single interferogram has long been of interest, despite its limitations in detecting large constant phases and distinguishing between the concave and convex profile shapes. However, this method remains valuable for applications focused on relative phase changes and their models [1, 2], where adjustments can be made to the constant phase and curvature sign. For such applications, the trade-off between experimental setup complexity and phase recovery typically favors the latter due to challenges in obtaining even a basic single interferogram. The key goal here is to recover a two-dimensional (2D) phase profile with a maximum number of nodes for further modeling of the material characteristics [1, 2]. This process involves the following steps: obtaining the interferogram, recovering the phase (adjusting curvature sign as needed), converting it to optical path difference (OPD), and fitting the OPD profile to describe material or geometrical parameters. The accuracy of these parameters depends on the quality of fitting, which explains the need for the high number of nodes in the OPD profile. This requires access to all pixels available in the interferogram, thus framing the problem of recovering the phase per pixel.

Currently, two main approaches exist for recovering the phase profile from a single interferogram. The first one uses the wrapped discrete  $2\pi$ -phase pieces from the interferogram, leading to the  $2\pi$  discontinuity problem. This issue is addressed by algorithmic methods that unwrap the phase for each piece individually – the *piecewise phase unwrapping* (PPU) approach [3, 4]. The second one, operating with the already unwrapped continuous phase – the *continuous phase unwrapping* (CPU) approach, is represented by a single method which involves simulating

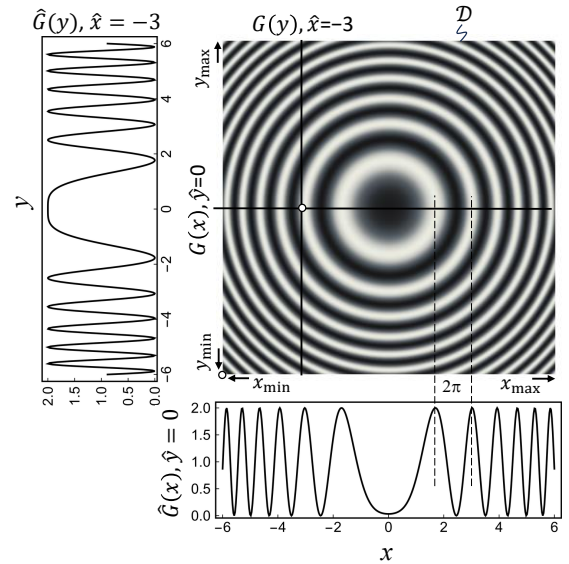


**Fig. 1.** The interferogram of the Example-1. Two 1D functions  $\hat{G}(x) = G(x, 0)$  and  $\hat{G}(y) = G(-3, y)$  represent two cross-sections intersecting at  $(-3, 0)$  denoted by the white point in the interferogram.  $D$  represents the interferogram boundary. The value  $G_{00} = G(-6, -6) = 2.0$  for computing  $\Theta_{00}$  is in the lower-left corner denoted by the white point.

the entire 3D wavefront interference to represent the interferogram. This method employs the 3D partial derivative transport intensity equation (TIE) for the unknown phase and solves it [5].

We extend the CPU approach by developing an alternative to TIE mathematical method that bypasses both the discontinuities inherent in PPU methods and the need to simulate the 3D wavefront for solving TIE. Our method employs 1D first-order ordinary differential equations (ODEs) for the interferogram function and the unknown continuous unwrapped phase. The interferogram function is derived from a single interferogram. Below, we present this new CPU method and provide analytical and numerical examples for demonstration.

**General definitions.** An interferogram is an image displaying a pattern of bright (constructive) and dark (destructive)

fringes resulting from interference, see Fig. 1. The fringe pattern is analyzed within a Cartesian coordinate system and is characterized by the gray values  $G(\mathbf{r})$  of the image pixels  $\mathbf{r} = (x, y)$ . These gray values oscillate between minimum (black) and maximum (white) pixel intensities in a region within a boundary  $\mathcal{D} = \{(x, y) : x_{\min} \leq x \leq x_{\max}, y_{\min} \leq y \leq y_{\max}\}$ , see Fig. 1. The function  $G(\mathbf{r})$  contains an information of a phase difference  $\theta(\mathbf{r})$  over the interferogram.

Following reference [3], consider a general form of the function  $G$ , suitable for the interference experiment where a single-pass object beam in free space produces interference fringes of infinite width, as illustrated in Fig. 1. The fringe pattern to be analyzed is

$$G = A + B \cos \theta, \quad (1)$$

where the gray function  $G$ , the coefficients  $A$  and  $B$ , and the phase  $\theta$  are the functions of a particular point  $(x, y)$  in the interferogram. While  $G$  is oscillating in space, the coefficients  $A$  and  $B$  are slowly varying functions of spatial coordinates [3]. Depending on the experimental conditions the coefficients  $A$  and  $B$  represent a background illumination and an amplitude of the recorded light modulation and we set them to constants.

**CPU method.** Consider an arbitrary 2D interferogram obtained in an experiment defined by Eq. (1). This interferogram represents a gray function  $G(\mathbf{r})$  defined in the region bounded by  $\mathcal{D}$ . Introduce the interferogram function  $F(\mathbf{r})$  – a relationship between the phase difference  $\theta(\mathbf{r})$  and the gray function  $G(\mathbf{r})$ , obtained from the specified experimental conditions. Rewrite Eq. (1) to obtain  $F$

$$\cos \theta(x, y) = F(x, y) = (G(x, y) - A)/B, \quad (2)$$

which also holds for the boundary  $\mathcal{D}$ . Differentiating Eq. (2) with respect to  $x$  and  $y$  we find

$$-\theta'_x \sin \theta = F'_x, \quad -\theta'_y \sin \theta = F'_y, \quad (3)$$

where  $f'_x = \partial f(x, y)/\partial x$  and  $f'_y = \partial f(x, y)/\partial y$ , respectively. Use Eqs. (2,3) in Pythagorean identity  $\sin^2 \alpha + \cos^2 \alpha = 1$  to eliminate the trigonometric functions from consideration and obtain

$$(\theta'_x)^2 = (F'_x)^2/(1 - F^2), \quad (\theta'_y)^2 = (F'_y)^2/(1 - F^2), \quad (4)$$

that can be solved independently. The method of solution is identical for both equations in Eq. (4), below we give a solution for the  $\theta'_x$  component only.

In Eq. (4) for the component  $\theta'_x$ , the coordinate  $y$  is a parameter, setting it to a specific value  $y = \hat{y}$  turns  $G, F$ , and  $\theta$  into the functions of the single variable  $x$ , namely  $\hat{G}(x) = G(x, \hat{y})$ ,  $\hat{F}(x) = F(x, \hat{y})$ , and  $\hat{\theta}(x) = \theta(x, \hat{y})$  which are defined over the interval  $x_{\min} \leq x \leq x_{\max}$ , where  $x_{\min}$  and  $x_{\max}$  values are taken from the boundary of the interferogram, see Fig. 1. A version of Eq. (4) written for the component  $\theta'_x$  with a single variable  $x$  reads

$$(\hat{\theta}'_x)^2 = (\hat{F}'_x)^2/(1 - \hat{F}^2). \quad (5)$$

Eq. (5) is 1D ODE of the first-order with the already unwrapped phase. For representing the 2D profile of the phase, create  $K$  functions  $\hat{F}_k(x)$  taken from the interferogram pattern for a set  $Y = \{\hat{y}_k : 1 \leq k \leq K\}$  of values  $y_{\min} \leq \hat{y}_k \leq y_{\max}$ . In this case, Eq. (5) generates a series of phase profiles denoted as  $\hat{\theta}_k(x) = \theta(x, \hat{y}_k)$ . Solution of this equation for the profiles  $\hat{\theta}_k(x)$  requires corresponding initial condition at the boundary  $x = x_{\min}$ , specifically  $\theta(x_{\min}, \hat{y}_k)$ .

To solve Eq. (5) apply the relations  $\sqrt{f^2} = |f|$  where  $|\cdot|$  denotes a modulus and  $|f(x)| = \text{sgn}(f) \cdot f \geq 0$  and  $\text{sgn}(\cdot)$  stands for the sign function returning  $\pm 1$ , and obtain

$$\hat{\theta}(x) = \Theta_{0y} + \text{sgn}(\hat{\theta}'(x)) \int_{x_{\min}}^x \frac{|\hat{F}'(\xi)| d\xi}{\sqrt{1 - \hat{F}^2(\xi)}}. \quad (6)$$

Here  $\Theta_{0y}$  denotes the boundary value  $\theta(x_{\min}, \hat{y}_k)$ , where the index 0 indicates the minimal value,  $x_{\min}$ , according to  $\mathcal{D}$ ;  $\Theta_{0y}$  can be found from Eq. (4, right) solving it along the  $y$ -axis for  $x = x_{\min}$ . The solution similar to Eq. (6) reads

$$\theta(x_{\min}, y) = \Theta_{00} + \text{sgn}(\theta'(x_{\min}, y)) \int_{y_{\min}}^y \frac{|F'(x_{\min}, \psi)| d\psi}{\sqrt{1 - F^2(x_{\min}, \psi)}}, \quad (7)$$

where  $\Theta_{00}$  denotes the boundary value  $\theta(x_{\min}, y_{\min})$  with the same convention for indices. Eq. (7) defines the boundary conditions for Eq. (6) with  $y = \hat{y}_k$ . The value of  $\Theta_{00}$  can be determined from Eq. (2)

$$\cos \Theta_{00} = F_{00} = (G_{00} - A)/B, \quad (8)$$

where  $F_{00} = F(x_{\min}, y_{\min})$ , with  $G_{00} = G(x_{\min}, y_{\min})$ . The value of  $G_{00}$  is taken from the lower-left corner of the interferogram, as it is shown in Fig. 1. Eq. (8) has two solutions for  $\Theta_{00}$  in the interval  $-\pi \leq \Theta_{00} \leq \pi$ . While both solutions satisfy the initial  $G(\mathbf{r})$  pattern, only one satisfies the experimental conditions. Since  $\Theta_{00}$  is a constant, it shifts the 2D phase profile  $\theta(x, y)$  as a whole. Thus, either solution of Eq. (8) will not affect the general shape of the phase.

In Eqs. (6,7), the integrand term at the first glance represents an indeterminate 0/0 for certain argument values. However, applying the l'Hospital's rule to the integrand quotient reveals that terms contributing to a (possible) divergence cancel out. The function  $\text{sgn}(\hat{\theta}'(x))$  could be obtained once the extremum points  $x_i$  of  $\hat{\theta}(x)$  are found from the equation  $\hat{\theta}'(x) = 0$ . As at these points both sides of Eq. (5) vanish, the equation for the extrema  $x_i$  reads

$$(\hat{F}'_x)^2/(1 - \hat{F}^2) = 0. \quad (9)$$

Eq. (9) can be written in the finite difference form by using the l'Hospital's rule and solved numerically, same is applied for the integrand in Eqs. (6,7). For a sequence of  $n$  roots  $x_i, 1 \leq i \leq n$ , of Eq. (9), the whole interval should be divided into a sequence of  $n + 1$  segments  $s_i : \{x_{i-1} \leq x \leq x_i\}, 1 \leq i \leq n + 1$ , where each segment is characterized by a specific value of sign  $\sigma_i = \text{sgn}(\hat{\theta}'(x))$  and  $x_{n+1} = x_{\max}$ . The sign alternates between the adjacent segments. Thus, the whole sign sequence is determined by  $\sigma_1$  in the first segment  $s_1 : \{x_0 = x_{\min} \leq x \leq x_1\}$  and it does not affect the generic shape of the unwrapped phase.

During computation, the integral of Eq. (6) is applied per segment  $s_i$  while the argument  $x \in s_i$ , then the phase at the end point  $x_{i-1}$  of the preceding segment  $\Theta_{i-1} = \theta(x_{i-1}, \hat{y})$  must be added. Thus, for the interval  $x_{i-1} \leq x \leq x_i$  the phase  $\hat{\theta}_i(x)$  reads

$$\hat{\theta}_i(x) = \Theta_{i-1} + \text{sgn}(\hat{\theta}'_i(x)) \int_{x_{i-1}}^x \frac{|\hat{F}'(\xi)| d\xi}{\sqrt{1 - \hat{F}^2(\xi)}}. \quad (10)$$

For solution along the  $y$ -axis, replace the variable  $x$  by  $y$  in the above 1D solution, while selecting  $x = \hat{x}_m$ . It outputs the stack of  $M$  profiles  $\hat{\theta}_m(y) = \theta(\hat{x}_m, y)$  of the phase. These profiles require the conditions  $\Theta_{x0} = \theta(\hat{x}_m, y_{\min})$  along the  $x$ -coordinate, ultimately leading to the same condition  $\theta(x_{\min}, y_{\min}) = \Theta_{00}$  determined from the interferogram, as done above.

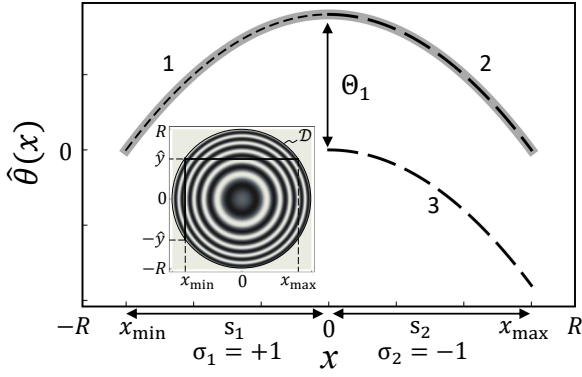


**Fig. 2.** Analytical example of 1D phase recovery. The black dashed curves 1 and 2 denote the phase  $\hat{\theta}_1(x) = \hat{R}^2 - x^2$  and  $\hat{\theta}_2(x) = \Theta_1 - x^2$  (with  $\Theta_1 = \hat{R}^2$ ) corresponding to the segments  $s_1$  and  $s_2$ , where  $x_{\min} = -\hat{R}$  and  $x_{\max} = \hat{R}$ , respectively. The black dashed curve 3 denotes the evaluation of the integral in Eq. (12). The parabolic gray curve unites both dashed curves denoting the resulting phase  $\hat{\theta}(x)$ . The insert shows the interferogram with circular boundary  $\mathcal{D}$  and the chord of interest  $\hat{y}$ .

In general, for each point  $(\hat{x}_m, \hat{y}_k)$  in the interferogram, our method delivers two orthogonal components of the phase profiles  $\hat{\theta}_k(x)$  and  $\hat{\theta}_m(y)$  by solving two independent 1D ODEs effectively representing 2D phase surface. Once the 2D profile of the phase difference  $\theta$  is recovered, then the 2D optical path difference (OPD) can be computed for the given refraction coefficient of the media and the wavelength.

**Analytical example.** To illustrate the method, consider the “seed” phase difference defined as 2D, even, parabolic function:  $\theta(x, y) = R^2 - x^2 - y^2$  with the boundary  $\mathcal{D} = \{(x, y) : R^2 - x^2 - y^2 = 0\}$ , where  $R$  is constant, Fig. 2 (insert). Consider the phase recovery task in 1D for an arbitrary chord  $-R \leq \hat{y} \leq R$  limited along the  $x$ -coordinate by  $x_{\min} = -\hat{R}$  and  $x_{\max} = \hat{R} = \sqrt{R^2 - \hat{y}^2}$ . Use Eq. (1) with same assumptions and obtain the gray function  $G(x) = A + B \cos(\hat{R}^2 - x^2)$ . The goal is to evaluate Eq. (5), find the phase, and compare it with the “seed”. The interferogram function is given by  $\hat{F} = \cos(\hat{R}^2 - x^2)$  leading to  $|\hat{F}'_x / \sqrt{1 - \hat{F}^2}| = 2|x|$ . Eq. (9) gives a condition for the roots  $4x^2 = 0$ . In the interval  $-\hat{R} \leq x \leq \hat{R}$  there is a single root  $x_1 = 0$ , being an extremum point of the phase function, so it produces only two constant sign segments. In the first segment  $s_1 : \{-\hat{R} \leq x \leq 0\}$  the sign  $\sigma_1 = +1$ , the integrand of Eq. (10) is  $2|x|$ , and the phase  $\hat{\theta}_1(x)$  for this interval reads

$$\hat{\theta}_1(x) = \sigma_1 \int_{-\hat{R}}^x 2|\xi| d\xi = \hat{R}^2 - x^2, \quad (11)$$

note,  $\Theta_{0y} = 0$  as well as  $\Theta_{00} = 0$ , because the phase vanishes at all points of the boundary  $\theta|_{\mathcal{D}} = 0$  significantly simplifying computation, Fig. 2. In the second segment  $s_2 : \{0 \leq x \leq \hat{R}\}$  we have  $\sigma_2 = -1$ , and the phase for this interval  $\hat{\theta}_2(x)$  evaluates following Eq. (10) to

$$\hat{\theta}_2(x) = \Theta_1 + \sigma_2 \int_0^x 2|\xi| d\xi = \Theta_1 - x^2, \quad (12)$$

where  $\Theta_1 = \hat{R}^2$  is the phase value at the end point  $x = 0$  of the preceding segment  $s_1$  computed from Eq. (11). Uniting the segments we obtain the final phase  $\hat{\theta}(x) = \hat{\theta}_1(x) \cup \hat{\theta}_2(x) = \hat{R}^2 - x^2$  for the entire interval  $-\hat{R} \leq x \leq \hat{R}$ . As  $\hat{R}^2 = R^2 - \hat{y}^2$

and  $\hat{y}$  is arbitrarily selected we conclude that the final 2D phase  $\theta(x, y) = R^2 - x^2 - y^2$  coincides with the “seed” phase. Fig. 2 illustrates the recovery procedure.

**Numerical examples.** The 2D examples were numerically tested using Mathematica 10.4, (Wolfram Research, Inc.) using the following procedure:

- Define the seed phase  $\theta_s$  in a rectangular region;
- Apply Eq. (1) and create an analytical  $G(x, y)$  function with  $A = B = 1$ , leading to  $G(x, y) = 1 + \cos \theta_s$  for all examples;
- Create arrays  $\{x_a, 1 \leq a \leq 201\}$  of 201 nodes and  $\{y_b, 1 \leq b \leq 21\}$  of 21 nodes, and convert  $G$  into the digital array  $\{G_{a,b}\}$ ; compute the digital values of interferogram functions  $\{F_{a,b}\}$ ;
- Interpolate  $\{F_{a,b}\}$  with splines along all  $x$ -nodes for each node  $y_b$  creating an array of the functions  $F(x, y_b)$ ;
- Create  $F(x_1, y)$  along  $y$ -nodes for the first  $x$ -node; use for  $F(x_1, y)$  Eq. (9) written for variable  $y$  to find all roots  $y_i$  (extrema), compute the segments  $s_i$  and set their signs  $\sigma_i$ ; then employ Eqs. (10) and (7,8) and reconstruct the phase  $\theta(x_1, y)$ , this is a boundary condition for reconstructing the phases  $\theta(x, y_b)$  for given  $y_b$  along  $x$ ;
- For reconstructing each  $\theta(x, y_b)$ , set the  $y$ -node  $y_b$  and for the selected  $F(x, y_b)$  solve Eq. (9) finding all roots  $x_i$  (extrema), the segments  $s_i$  and set signs  $\sigma_i$ ; then employ Eqs. (10) and (7,8) and obtain  $\theta(x, y_b)$  taking into account the boundary condition  $\theta(x_1, y_b)$ ; then change the  $y$ -node and repeat.

**Example-1** considers the parabolic seed phase  $\theta_s(x, y) = 72 - x^2 - y^2$  with the square boundary  $\mathcal{D} = \{(x, y) : -6 \leq x \leq 6, -6 \leq y \leq 6\}$  according to Fig. 3a. The node  $(-6, -6)$  provides  $\Theta_{00} = 0.0$  and two first-node arrays provide the phases at the boundaries  $\Theta_{0y} = \theta(-6, y)$  and  $\Theta_{x0} = \theta(x, -6)$ , respectively. There is a single root  $x_1 = 0.0$ , making two segments  $s_1 : \{-6 \leq x \leq 0\}$  and  $s_2 : \{0 \leq x \leq 6\}$  with the selected signs  $\sigma_1 = +1$  and  $\sigma_2 = -1$ . Fig. 3a demonstrates a phase recovery along  $x$  and  $y$  directions corresponding to  $\theta(-3, y)$  and  $\theta(x, 0)$  phase components for the node  $\theta(-3, 0)$ .

**Example-2** illustrates the numerical recovery of the saddle type of the seed phase  $\theta_s(x, y) = x^2 - y^2$  with the square boundary  $\mathcal{D} = \{(x, y) : -6 \leq x \leq 6, -6 \leq y \leq 6\}$ . 21 profiles  $\theta(x, y_b)$  are recovered producing an effective approximation of 2D phase surface. The corresponding interferogram is presented in Fig. 3b. The boundary conditions for the  $\theta(x_{\min}, y_{\min})$  and the first  $y$ -node are following:  $\Theta_{00} = \theta(-6, -6) = 0.0$  and  $\Theta_{0y} = \theta(-6, y_b)$ , respectively. There is a single root  $x_1 = 0.0$  along both directions, providing for each two segments of integration  $s_1$  and  $s_2$ , having different signs  $\sigma$ . Along the  $x$ -axis  $s_1$  has  $\sigma_1 = -1$ , while along the  $y$ -axis  $s_1$  has  $\sigma_1 = +1$ . Signs are selected by trials in order to match the recovered phase with the initial seed phase.

**Example-3** recovers the phase from the pit-and-hill interferogram, Fig. 3c. The interferogram corresponds to the seed phase  $\theta_s(x, y) = 1 + 50x \exp(-(0.4x + 0.3)^2 - (0.3y)^2)$  with the square boundary  $\mathcal{D} = \{(x, y) : -6 \leq x \leq 6, -6 \leq y \leq 6\}$ . The phase was recovered along  $x$ -axis  $\theta(x, y_b)$  represented by 21 curves aligned with the 2D profile of  $\theta_s$  in Fig. 3c. The value  $\Theta_{00} = \theta(-6, -6)$  is 0.857; the boundary conditions for each  $\theta(x, y_b)$  is  $\Theta_{0y} = \theta(-6, y_b)$  shown in the Fig. 3c insert. Solution



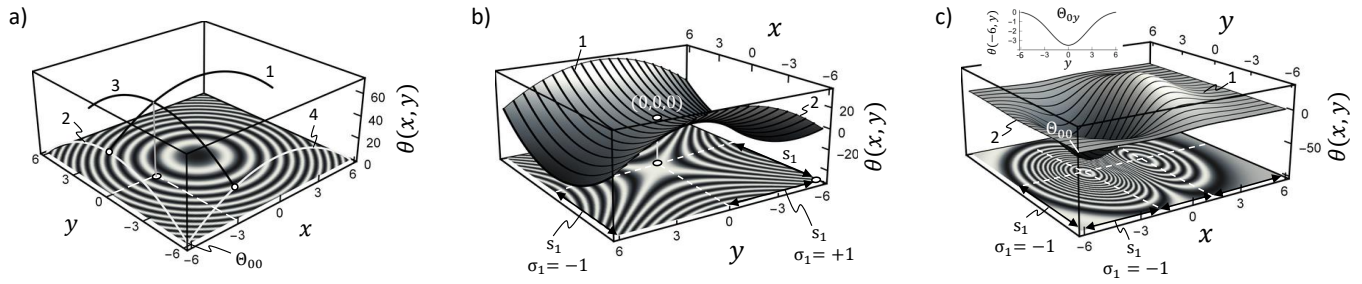


**Fig. 3.** Numerical recovery of phase from the interferogram having a) parabolic (Example-1), b) saddle (Example-2) and pit-and-hill (Example-3) type of the fringe pattern. a) Two orthogonal phase components are recovered. The black thick curves labeled 1 and 3 represent the numerical solutions  $\theta(x,0)$  and  $\theta(-3,y)$  of Eq. (6). The white vertical line is a projection of the phase components' intersection and the node of interest  $(-3,0)$  in the interferogram. White curves 2 and 4 are the boundary conditions  $\Theta_{0y}$  and  $\Theta_{x0}$ , respectively. In b) and c) 2D shape is constructed by 21 curves  $\theta(x,y_b)$  recovered along  $x$ -direction, with typical profile denoted by 1. The curve of the boundary conditions  $\Theta_{0y}$  for each  $\theta(x,y_b)$  is marked by 2. Only the first segment  $s_1$  and its sign  $\sigma_1$  are shown for both  $x$  and  $y$  directions. In c) 2 denotes the curve of the boundary conditions  $\Theta_{0y}$  shown in the insert for clarity.

of Eq. (9) gives two roots along the  $x$ -axis  $(-2.182, 1.432)$  corresponding to the extrema and providing three segments  $s_1, s_2$  and  $s_3$  for integration in Eqs. (6,7,10); the sign for  $s_1$  is selected  $\sigma_1 = -1$ . There is one root  $x_1 = 0.0$  along the  $y$ -axis providing two segments  $s_1, s_2$ ; the sign for  $s_1$  is selected  $\sigma_1 = -1$ . Both  $\sigma_1$  are selected by trials to match the initial phase seed (in practice the experimental insights must be used). Recovering the phase along  $y$ -axis produces the  $\theta(x_a, y)$  curves require changing the sign of  $\sigma_1$  while progressing along  $x_a$  nodes.

**Discussion.** In summary, our method allows to recover 2D phase profile from a single interferogram by analyzing fringe patterns of different complexity. The user defines the interferogram function  $F$ , manages the constant phase matching  $-\pi \leq \Theta_{00} \leq \pi$ , and initializes the sign  $\sigma_1$  for the first integration segment  $s_1$ . The method outputs the recovered phase profile. To align with the interferogram and/or experimental conditions, the user may need to change the sign of  $\sigma_1$  and remove the numerically computed roots corresponding to the inflection points along the integration path, addressing the inherent insensitivity of the interferogram pattern to the phase profile concavity or convexity.

For complex patterns with varying phase curvature, the method accurately tracks the phase profile changes along the integration path taken parallel to the line connecting the phase profile extrema in the interferogram.

If the media where interference occurs have refractions and the interfering wavefronts have reflections, the functions  $G$  and  $F$  differ from those in Eqs. (1,2). The preprint [6] provides an example of phase recovery using this new method in the more complex case involving experimental interference in thin liquid films, which is applicable to the contexts described in [1, 2]. The presented novel CPU method of continuous phase unwrapping can be considered as a complementary one to the existing PPU and CPU-TIE methods.

**Disclosures.** The authors declare no conflicts of interest.

**Data availability.** Data underlying the results of this paper is presented in this paper.

## REFERENCES

1. P. Dell'Aversana, V. Tontodonato, and L. Carotenuto, Suppression of coalescence and of wetting: The shape of the interstitial film, *Phys. Fluids* **9**, 2475 (1997).
2. S.J. Gokhale, J.L. Plawsky, P.C. Wayner, *et al*, Inferred pressure gradient and fluid flow in a condensing sessile droplet based on the measured thickness profile, *Phys. Fluids* **16**, 1942 (2004).
3. T.R. Judge and P.J. Bryanston-Cross, A review of phase unwrapping techniques in fringe analysis, *Opt. Lasers Eng.* **21**, 199 (1994).
4. D. Malacara, M. Servín, and Z. Malacara, "Interferogram Analysis for Optical Testing," in *Interferogram Analysis for Optical Testing*, 2nd ed. (Taylor & Francis Group, 2005), p. 546.
5. N. Pandey, A. Ghosh, and K. Khare, Two-dimensional phase unwrapping using the transport of intensity equation, *Appl. Opt.* **55**, 2418 (2016).
6. V. Berejnov and D. Li, A simple method of measuring profiles of thin liquid films for microfluidics experiments by means of interference reflection microscopy, arXiv1006.2180 (2010).